THE JOURNAL OF PROSTHETIC DENTISTRY

RESEARCH AND EDUCATION

Microstructural and mechanical characterization of six Co-Cr alloys made by conventional casting and selective laser melting

Youssef S. Al Jabbari, BDS. MS. PhD. FACP,[a] Konstantinos Dimitriadis, CDT, PhD,[b] Aref Sufyan, BS,[c] and Spiros Zinelis, BEng, PhD[d]

ABSTRACT

Statement of problem. Three Co-Cr alloy types (Co-Cr-Mo, Co-Cr-W, and Co-Cr-Mo-W) have been commonly used in the fabrication of dental prostheses. These alloys can be manufactured using either conventional casting or selective laser melting (SLM) techniques. Nevertheless, research that directly compares these materials and/or manufacturing processes in terms of their microstructural and mechanical characteristics is sparse.

Purpose. The purpose of this in vitro study was to conduct microstructural and mechanical analysis via X-ray interpretation, optical microscopy, scanning electron microscopy/energy dispersive X-ray spectroscopy (SEM/EDS), image analysis, X-ray diffraction (XRD), instrumented indentation testing (IIT), and 3-point bending testing to characterize Co-Cr-Mo, Co-Cr-W, and Co-Cr-Mo-W alloys produced through conventional casting and SLM.

Material and methods. Six Co-Cr-based alloys were analyzed and divided into 3 types based on their elemental composition (Co-Cr-Mo, Co-Cr-W, and Co-Cr-Mo-W). Additionally, each group was categorized based on the manufacturing process used (casting or SLM). X-ray scans were used to assess porosity. The microstructures of the specimens were assessed through SEM/EDS examination and XRD analysis. IIT was used to determine the Martens hardness (HM) and elastic index (η_{IT}), while the elastic modulus (E) was estimated through the 3-point bending test. The mechanical properties were statistically analyzed using 2-way analysis of variance (ANOVA) and the Tukey multiple comparison post hoc test, with alloy type and manufacturing process as discriminating variables (α=.05).

Results. All cast groups exhibited gross porosity, while no pores or other flaws were found in the SLM groups. Based on the XRD results, the crystalline structure of all Co-Cr specimens consisted of the face-centered cubic γ phase (γ-fcc), along with the hexagonal close-packed ε phase (ε-hcp) and $Cr_{23}C_6$ carbide. Different microstructures were identified between the cast and SLM alloys. Significant differences were identified for the mean standard deviation HM (ranging from 2601 ±94 N/mm^2 to 3633 ±61 N/mm^2) and mean ±standard deviation η_{IT} (ranging from 16.8 ±0.3% to 20.9 ±0.3%) among alloys prepared by the same manufacturing process, while all SLM alloys had statistically higher HM and η_{IT} results than their cast counterparts (P<.05). No statistically significant differences were identified for the mean ±standard deviation E_b (ranging from 170 ±25 GPa to 244 ±36 GPa) among the groups prepared with the same manufacturing process (P>.05), but the SLM alloys had significantly higher results (P<.05) than the cast alloys.

Conclusions. In general, the manufacturing procedure significantly affected the porosity, microstructure, and mechanical properties of the tested Co–Cr alloys. SLM decreased the internal porosity, provided a uniform microstructure, and improved the mechanical properties for all the tested alloy types. (J Prosthet Dent 2024;132:646.e1-e10)

Supported by the Vice Deanship of Scientific Research for Research Chairs, Saudi Arabia.
No conflict of interest.

[a]Director, Dental Biomaterials Research and Development Chair and Professor, Prosthetic Dental Sciences Department, College of Dentistry, King Saud University, Riyadh, Saudi Arabia.
[b]Research fellow, Department of Biomaterials, School of Dentistry, National and Kapodistrian Universty of Athens, Athens, Greece.
[c]Researcher, Dental Biomaterials Research and Development Chair, College of Dentistry, King Saud University, Riyadh, Saudi Arabia.
[d]Professor, Department of Biomaterials, School of Dentistry, National and Kapodistrian Universty of Athens, Athens, Greece and International Professor of Dental Biomaterials Research and Development Chair, King Saud University, Riyadh, Saudi Arabia.

Clinical Implications

SLM alloys exhibit minimal internal porosity, an advantageous microstructure, and favorable mechanical properties; thus, improved clinical efficacy is anticipated with the use of the SLM manufacturing process.

The development of cobalt chromium (Co-Cr) alloys can be traced back to groundbreaking research in 1913 when their remarkable strength and resistance to staining were discovered and molybdenum (Mo) and tungsten (W) were found to be effective strengthening alloying elements.[1] Co-Cr alloys exhibit a high strength and elastic modulus, excellent wear resistance,[2] excellent biocompatibility,[3] and corrosion and tarnish resistance,[2,4–6] leading to biomedical applications. Co-Cr alloys were first utilized in dentistry during the 1930s to produce removable partial denture (RPD) frameworks, and the use of Co-Cr-based alloys as metal–ceramic materials was described in 1959.[2,7]

The elemental composition of Co-Cr alloys is specified in the ASTM F75–18 standard[8] for orthopedic and dental surgical implants made of Co-Cr-Mo alloy. The Cr content should range between 27 and 30 wt%, the Mo content should be between 5 and 7 wt%, and the W content should not exceed 0.2 wt%. Co-Cr alloys for the manufacture of RPDs and metal–ceramic restorations have different specifications. According to the 1987 version[9] and 1994 version of the International Organization for Standardization (ISO) 6871–1 standard[10] for an RPD Co-Cr alloy, the combined mass of Co and Cr should be greater than 85 wt%, with Cr comprising at least 25% and Mo comprising at least 4 wt%. For metal–ceramic restorations, the ISO 9693 standard[11] does not impose any specific restrictions on the elemental composition of the alloys and allows W as the primary alloying element instead of or in combination with Mo after Cr. The adoption of the ISO 22674[12] standard in 2006 categorized dental alloys based on their mechanical properties and application, eliminating the previous restrictions regarding elemental compositions.

Recently, the production of dental metallic prostheses has changed from the traditional lost-wax casting process to computer-aided design and computer-aided manufacturing (CAD-CAM),[13–16] including additive technologies such as selective laser melting (SLM).[17–19] Modifications in either the elemental composition or fabrication techniques for Co-Cr alloys have resulted in alterations in their physical properties,[17,20–31] leading to differences in their mechanical[20,32] and electrochemical properties,[33,34] as well as in their biocompatibility.[4,35–37]

The mechanical properties of alloys, as specified by the ISO 22674 standard,[12] are essential for determining their suitability for use in dental prostheses. In the case of metal–ceramic restorations, the successful bonding of porcelain to the alloy relies heavily on the physicomechanical properties of the metal substructure.[38] As RPDs undergo significant dynamic forces during mastication and insertion and removal by the patient, high stiffness and strength are required,[39,40] with clasp failure recorded as the most common complication of RPDs, typically after 5 to 6 years of use.[41]

Three types of Co-Cr alloys are currently used for fabricating dental prostheses, classified based on the presence of Mo and/or W[4,23,42–46]: Co-Cr-Mo, Co-Cr-W, and Co-Cr-Mo-W. Thus, the aim of this study was to conduct a microstructural and mechanical characterization of Co-Cr-Mo, Co-Cr-W, and Co-Cr-Mo-W alloys produced through conventional casting and SLM. The null hypotheses were that no significant differences would be found among different alloy types or between the different manufacturing processes.

MATERIAL AND METHODS

Six Co-Cr-based alloys for the manufacturing of metal–ceramic crowns and fixed partial dentures were included in this study, as shown in Table 1. The first part of the group names represents the alloying system (Mo, W, and MoW, respectively), and the second part represents the manufacturing process (C for casting and L for SLM).

For each group, 20 rectangular specimens with dimensions of 25×3×0.45–0.55 mm were prepared. The cast group specimens (Mo-C, W-C, and MoW-C) were prepared using the traditional casting procedure with a centrifugal casting machine (Ducatron S3; UginDentaire). The Mo-L, W-L, and MoW-L specimens were manufactured by using SLM devices (PM 100 Dental System; Phenix Systems, Mlab; ConceptLaser, EOS Laser Sintering M270; EOS). A thorough description of the manufacturing process and materials used have been reported previously.[4] The specimens were ground on all surfaces up to 1200-grit SiC paper under continuous water cooling to final dimensions of 25×3×0.45–0.55 mm in a grinding polishing machine (Dap V; Struers).

After metallographic finishing, all specimens were tested with a dental X-ray unit (Orix 70; Ardet) operating at 70 kV, 5 mA, and an exposure time of 0.35 seconds. Digital images were checked by the unaided eye. The ground surfaces were imaged using an automated digital light microscope (DM4000B; Leica).

The crystalline phases were characterized by X-ray diffraction (XRD) (D8 Advance; Bruker); Cu Kα radiation (λ=1.5406 Å) was used, which was produced at 30 kV and 25 mA. Diffraction angles (2θ) between 30 and 110 degrees were scanned at a rate of 0.005 degrees/second.

Table 1. Brand names, elemental compositions (as provided by manufacturers), manufacturing methods, and group names of materials tested

	V-Comp[a]	ST2724G[b]	Remanium Star[c]	Remanium StarCL[c]	Wirobond 280[d]	EOS-CobaltChrome SP2[e]
Co	61.1 ±2	62.5 (min)	60.5	60.5	60.2	61.8-65.8
Cr	32 ±2	29	28	28	25	23.7-25.7
Mo	5.5 ±1	5.5			4.8	4.6-5.6
W			9	9	6.2	4.9-5.9
Si	<1	<1	1.5	1.5	<1	0.8-1.2
Mn	<1	<1		<1	<1	<0.1
Fe		<1				<0.5
Nb				<1		
Ga					2.9	
N				<1		
Lot number	N001535	16D0296	1122	25686	14073	H301601
Manufacturing process	Casting	SLM	Casting	SLM	Casting	SLM
Group name	Mo-C	Mo-L	W-C	W-L	MoW-C	MoW-L

[a] Dentsply, Elephant Dental
[b] SINT-TECH
[c] Dentaurum
[d] Bego
[e] EOS

Three rectangular specimens from each group were ground as described previously up to 4000 grit. The surfaces were then polished with diamond pastes (DP Paste; Struers) of 3-, 1-, 0.5- and 0.25=diamond grains in successive steps and immersed in an ultrasonic water bath for 5 minutes. Then, the specimens were analyzed by scanning electron microscopy (SEM) (Quanta 200; FEI). Backscattered electron images (BEIs) were acquired by using a 20-kV accelerating voltage, 102- μA beam current, 133 10^{-6} Pa chamber pressure, and ×500 nominal magnification (260×260 μm collecting window). Different phases and pores were identified based on the mean atomic number contrast, and pores were identified based on the gray contrast. Both were quantified with a dedicated image analysis software program (ESPRIT Feature, ESPRIT ver.1.9; Bruker).

Higher magnification BEIs were made for only the cast groups, as only the mean atomic contrast is provided in Figure 3. The BEIs were obtained under the same conditions, and X-ray maps of all probed elements were acquired after 15 minutes of acquisition. Spot analysis was also used to determine the elemental composition of each phase by collecting energy dispersive X-ray spectroscopy (EDS) spectra with a 200-second acquisition time. All EDS spectra were acquired using a spectrometer (Quantax; Bruker) attached to an SEM equipped with a slew-window silicon drift detector (X Flash 6|10; Bruker) and quantified by ESPRIT s/w in standardless mode employing atomic number, absorption, and fluorescence excitation (ZAF) corrective routines.

Finally, 1 spectrum was obtained from each alloy with a 5-kV accelerating voltage equal to the beam current (95 μA), acquisition time (200 seconds), ×500 nominal magnification (256×256 μm collecting window), and 1000 counts per second. A low KeV accelerating voltage was used to optimize the X-ray generation of light elements,[47] especially C, which plays a dominant role in the formation of carbides and thus the mechanical properties of Co–Cr alloys.[2]

Ten rectangular specimens from each group, embedded along their longitudinal axis in epoxy resin (Epofix; Struers), were ground and polished by following the same procedure and tested using instrumented indentation testing (IIT) and a universal hardness testing machine (ZHU0.2/Z2.5; Zwick Roell). Force indentation depth curves were acquired, and the Martens hardness (HM) and the elastic index (η_{IT}) were determined according to the International Organization for Standardization (ISO) 14577–1 specification.[48] The curves were recorded using a Vickers indenter with a 9.8-N force and 2-second dwell time.

Ten specimens from each group were subjected to 3-point bend testing with a crosshead speed of 1.5 mm/minute in a universal testing machine (Tensometer10; Monsanto). The bending elastic modulus (E_b) was calculated according to the formula: $E_b = \frac{L^3 \Delta P}{4bh^3 \Delta d}$, where.

L is the distance between the supporting rods (20 mm), b is the specimen width (3 mm), h is the specimen thickness (0.5 mm), and ΔP and Δd are the load and deflection increment, respectively, between 2 selected points in the elastic portion of the curve.

The results of all the mechanical properties were statistically analyzed by 2-way analysis of variance (ANOVA) and the Tukey multiple comparison post hoc test considering the alloy type and manufacturing process as discriminating variables (α=.05). All groups were initially checked for outliers with the Dixon Q test, followed by normality and equal variance tests with the Kolmogorov–Smirnov and Brown–Forsythe routines, respectively (α=.05). The statistical analysis was carried out with a software program (OriginPro; OriginLab Corp).

RESULTS

Representative X-ray images of specimens from all groups tested are presented in Figure 1. All cast groups exhibited gross porosity in the central region of the rectangular

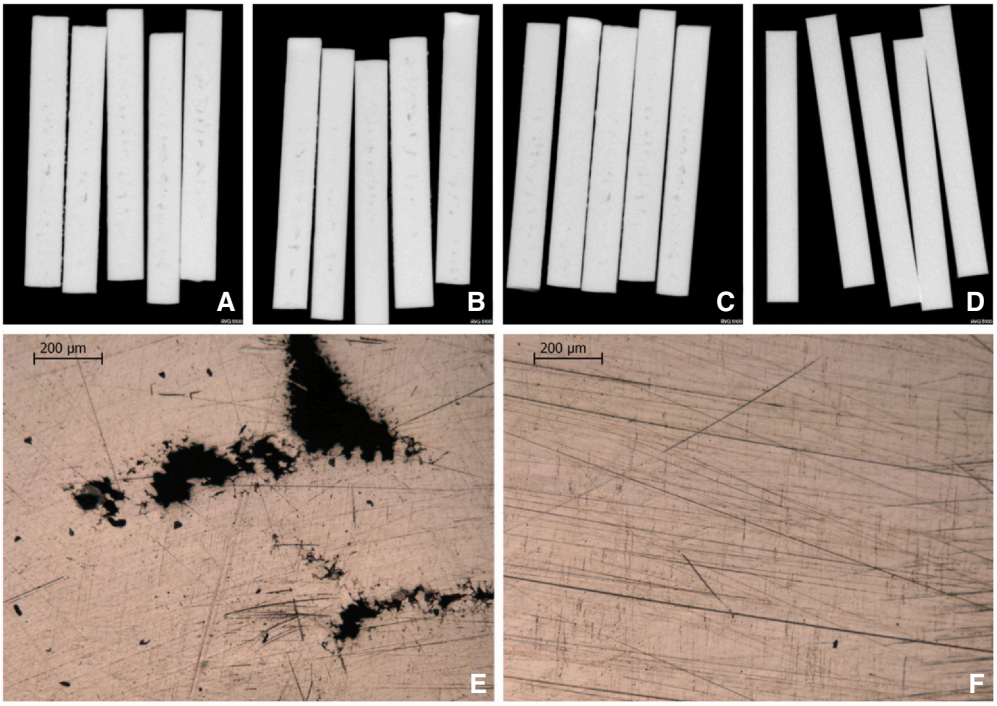

Figure 1. Porosity analysis of tested specimens. Representative X-ray images of cast groups (A: Mo-C; B: W-C; C: MoW-C; and D: Mo-L/W-L/MoW-L). 1E: Reflective light optical image from central region of rectangular specimen with gross porosity. 1F: Representative image of surface of specimens in selective laser melting groups.

specimens (Fig. 1A-C), while no pores or other flaws were found in the SLM groups (Fig. 1D). The central region of a representative cast specimen is shown in Figure 1E, where the pores are easily identified. In contrast, no defects other than surface lines from surface grinding were identified for the SLM specimens (Fig. 1F).

Figure 2 shows representative XRD patterns from all the groups tested, where in addition to the face-centered

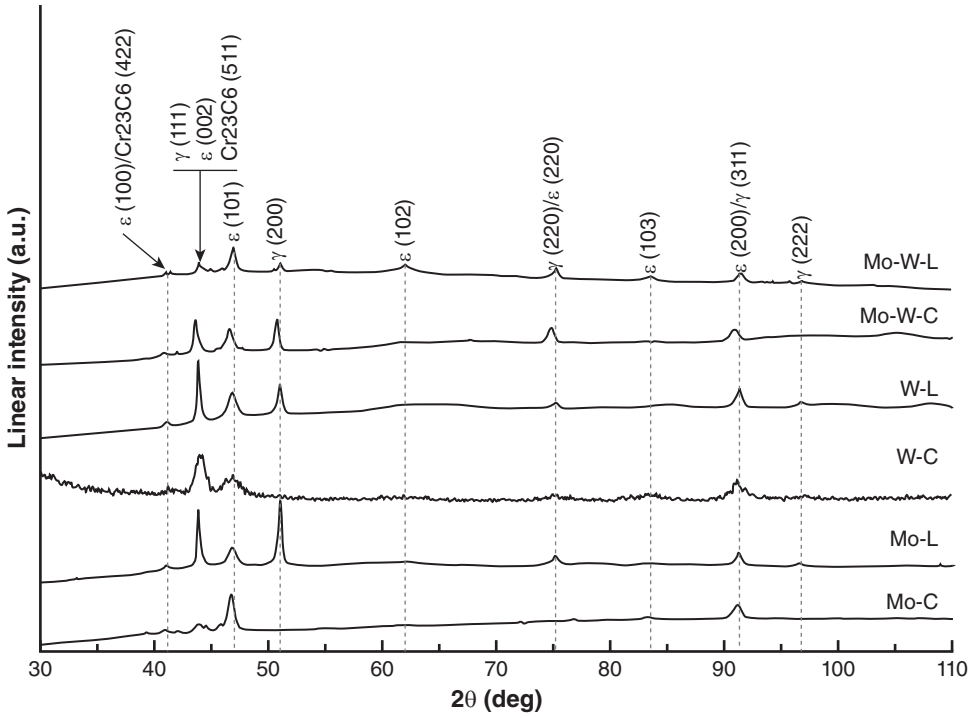

Figure 2. X-ray diffraction spectra from groups tested.

cubic γ phase (γ-fcc; 44.2 degrees, 51.5 degrees) of Co and Cr, the hexagonal close-packed ε phase (ε-hcp; 47.5 degrees, 92.5 degrees) of Co_3Mo was identified in all the specimens. Additionally, $Cr_{23}C_6$ carbide was identified in the cast and SLM groups.

Figure 3 shows the BEIs of all the groups tested. All cast groups showed a random distribution of small pores (Fig. 3A, C, E), but a few isolated pores can be identified in the SLM groups (Fig. 3B, D, F). In contrast with those in the cast groups (Fig. 3A, C, E), no difference in the mean atomic number was detected among the SLM groups (Fig. 3B, D, E). The steps of phase discrimination and calculation in image analysis are presented in Figure 3, and the percentage content of each phase is shown in Table 2.

The BEI and area mapping results are presented in Figure 4 for all cast groups, which show the inter-dendritic segregation of metallic elements. For Mo-C, the distribution of Mo is complementary to that of Co

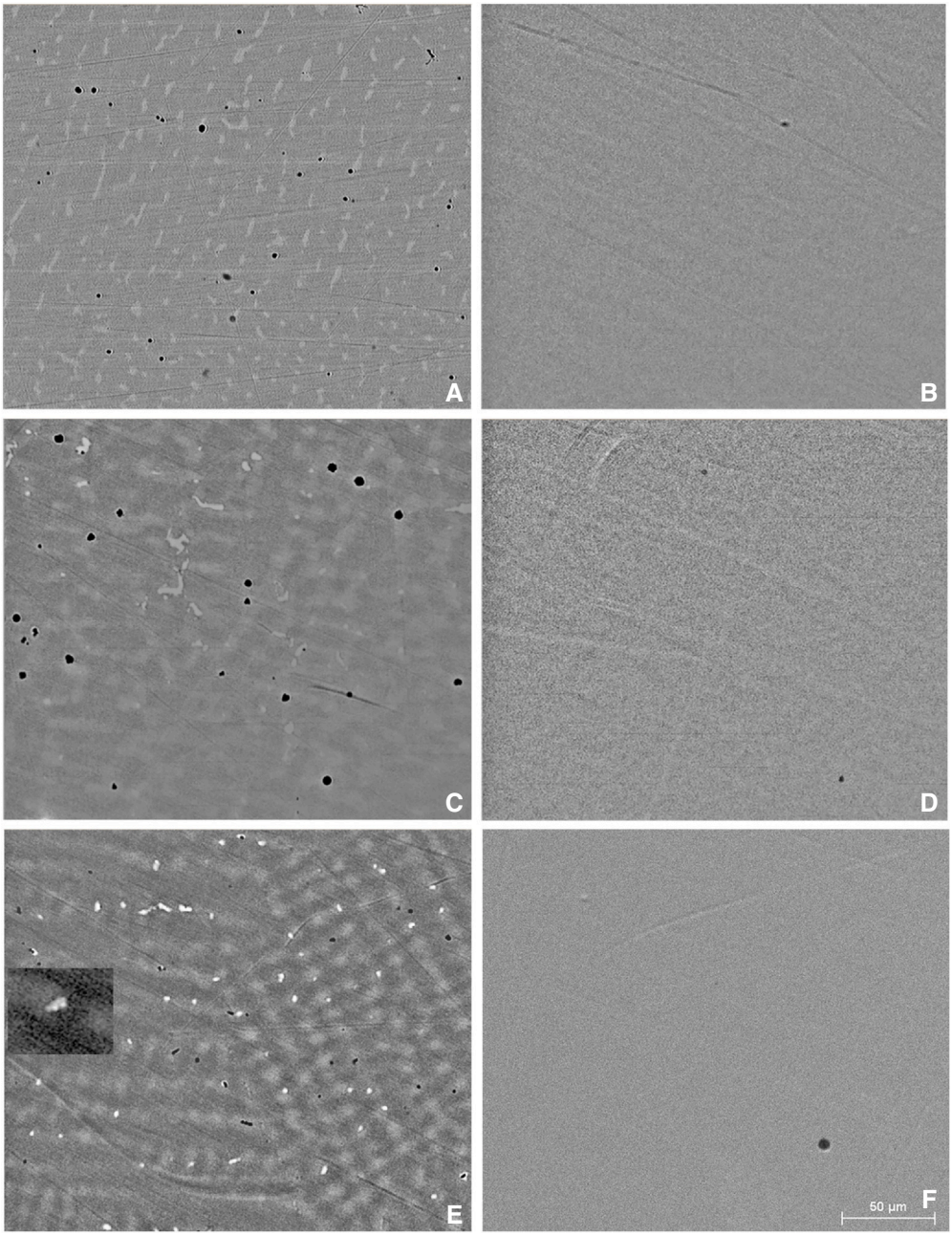

Figure 3. Representative backscattered electron images from all groups tested. Mean atomic number contrast evident for all cast groups (A, C, and E) but absent for selective laser melting groups. Mo-C (A) shows a diffuse second phase, and W-C (C) shows 2 diffuse phases. MoW-C (E) shows 3 additional phases apart from matrix, as illustrated in inset (E) (clearer representation of these very small phases presented in Fig. 5D). Original magnification ×500 (scale shown only in F for sake of clarity).

Table 2. Percentages ±standard deviation of microporosity, matrix, and distributed phases (ID: interdendritic phase) in all groups after quantification by image analysis (n=3)

Group	Microporosity	Matrix	ID 1	ID 2	ID 3
Mo-C	0.5 ±0.2	90.3 ±0.4	9.2 ±0.5		
Mo-L	0.2 ±0.1	99.8 ±0.1			
W-C	0.4 ±0.2	70.3 ±1.8	26.0 ±0.6	3.3 ±1.4	
W-L	0.2 ±0.1	99.8 ±0.1			
MoW-C	0.4 ±0.1	71.4 ±0.2	27.1 ±0.3	0.8 ±0.1	0.3 ±0.1
MoW-L	0.2 ±0.1	99.8 ±0.1			

ID1, interdendritic phase 1; ID2, interdendritic phase 2; ID3, interdendritic phase 3

and seems to follow the bright areas of the BEI (Fig. 5A). The same is true for W-C, where W and Nb show a complementary distribution to Co (Fig. 5B). In Figure 5C, Mo and W have complementary distributions to Co (Cr has a homogeneous distribution and is omitted for the sake of further clarifying the W-C and MoW-C groups). At higher magnification, for the MoW-C alloy, Cr shows a partially complementary distribution to Co and Mo, and W shows a complementary distribution to Co following the presence of mean atomic number contrast phases in a BEI. The elemental composition of each phase after EDS spot analysis is presented in Table 3. Figure 6 shows the overlapping EDS spectra of all the materials tested, acquired at an accelerating voltage of 5 keV and equivalent background signals, whereas Mo-C and Mo-L show more intense C peaks than the other materials.

Significant differences were identified for HM (P<.001) and η_{IT} (P<.001) among alloys prepared by the same manufacturing process, while all alloys showed statistically higher HM and η_{IT} than their cast counterparts (Table 4). No statistically significant differences were identified for E_b among the cast and SLM groups (P>.05) prepared with the same manufacturing process, but all the SLM alloys exhibited a higher E_b (P<.001).

DISCUSSION

The null hypothesis that no significant differences would be found among different alloy types or between the different manufacturing processes was rejected, as significant differences were identified among the materials tested. The presence of gross porosity (Fig. 1A-C) in all cast groups was consistent with previous studies[20,29,30,37] and is attributed to the dendritic structure of Co-Cr alloys, where, during solidification, the space among dendrites is easily isolated from the melt, resulting in pore formation.[29,30] All cast alloys exhibit the same limitation, and thus, differences in formulation have no effect on the development of internal porosity. In contrast, all specimens from the SLM groups were found to be free of large pores and internal flaws, consistent with previous reports.[18,19,37] Under high magnification (Fig. 3), all groups revealed the presence of spherical micropores at percentages lower than 0.5%, consistent with previous studies, at least for the Co-Cr-Mo alloys.[37] The presence of spherical micropores is a common finding, attributed to gas entrapment in the liquid metal during casting and in the molten pool during the SLM procedure.[37] These findings suggest that the elemental composition of the alloys did not affect the development of internal porosity. However, the manufacturing process plays a significant role in eliminating gross porosity as seen in the 4 tested SLM groups, implying that this manufacturing process successfully addressed the inherent limitations associated with the solidification mechanism of Co-Cr alloys during casting.[21,40]

The XRD results (Fig. 2) revealed that all alloys consisted of the γ-fcc phase, along with the ε-hcp phase and $Cr_{23}C_6$ carbides, consistent with previous findings.[14–16,33,39,45] The unstable γ-fcc structure dominates the structure of Co-Cr alloys at room temperature because of the slow reaction rate of the fcc ↔ hcp transformation, while the γ phase tends to transform to ε under the thermal treatment of stress relief annealing and porcelain firing.[23,46] However, in most situations, γ is the predominant phase, and the ε phase sometimes prevails.[32,43] Additionally, precipitates such as $Cr_{23}C_6$ carbides, which are the dominant carbides in cast and SLM Co-Cr alloys, were identified in all the Co-Cr specimens, consistent with previous studies.[22,23,31]

Image analysis revealed that the content of the interdentric phase in Mo-C was similar to previously

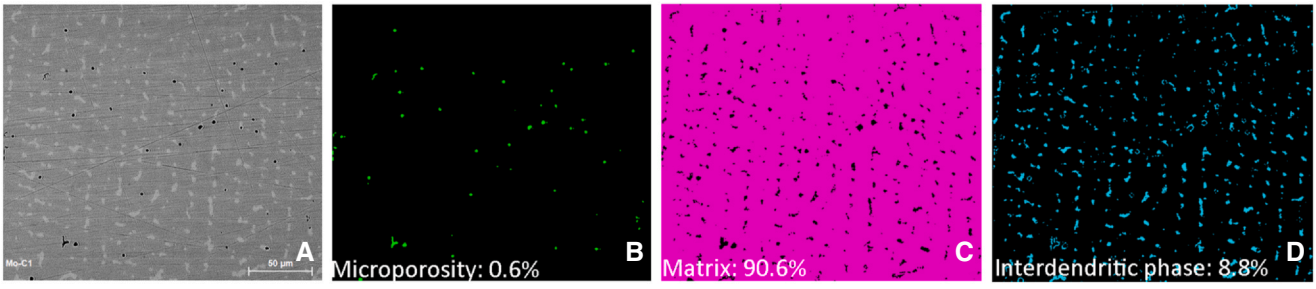

Figure 4. Representative images from phase analysis procedure. A, Backscattered electron image. B, Microporosity discriminated from remaining structure. C, Only matrix shown. D, Interdendritic phase.

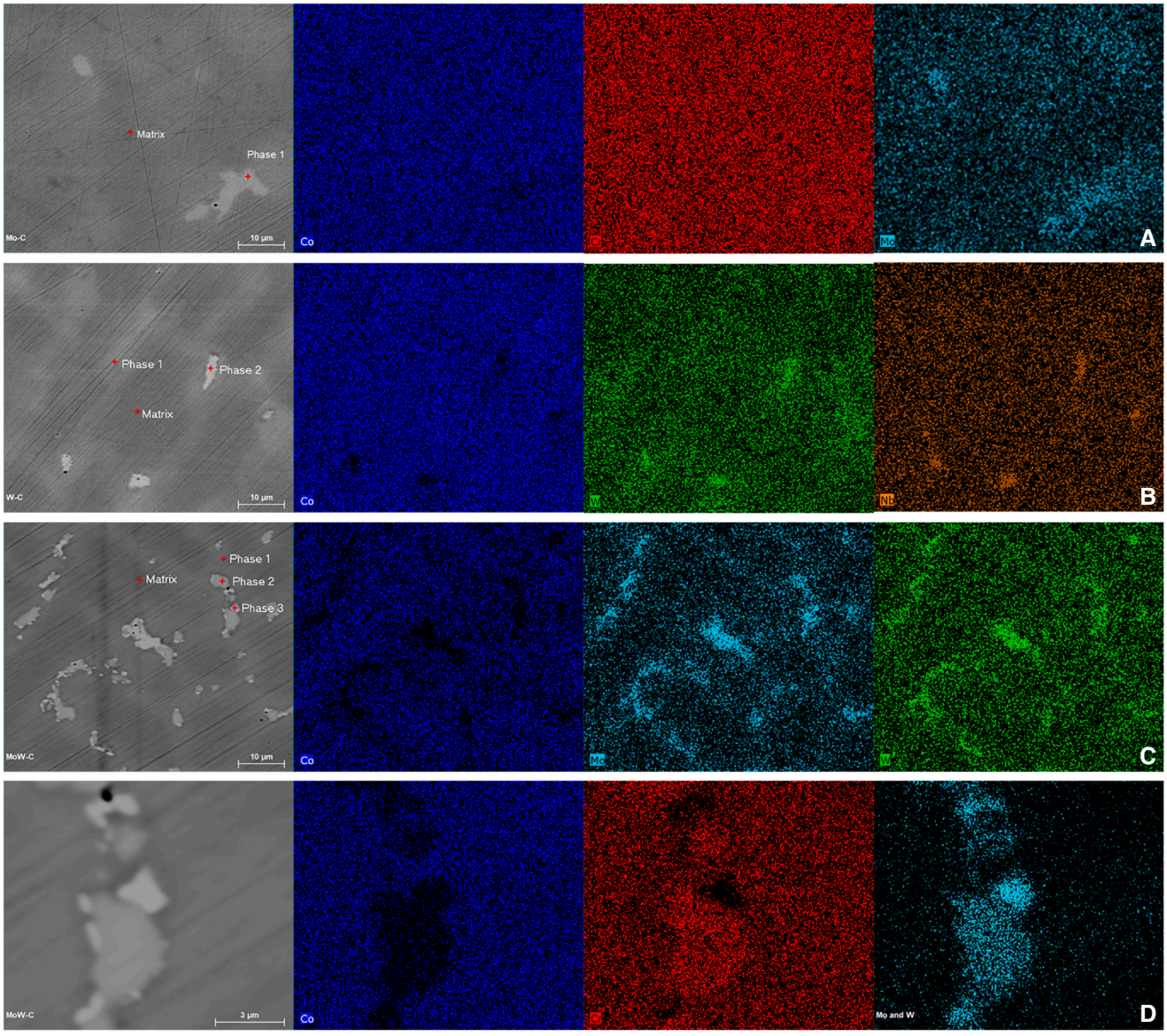

Figure 5. A: BEIs and corresponding energy dispersive X-ray spectroscopy elemental maps for Co, Cr, and Mo of Mo-C. B: Same for Co, W and Nb of W-C. The elemental map of Cr showed a homogeneous distribution and was omitted. C: BEIs and area mapping for Co, Mo, and W of MoW-C. The elemental map of Cr showed a homogeneous distribution and was omitted. D: Higher magnification images of Co, Cr, Mo, and W in MoW-C. Red crosses in BEIs indicate spot analysis points. Original magnification ×2000 for A, B, and C and ×10000 for D. BEIs, backscattered electron images.

reported values (7.2 ±0.3).[37] W-C and MoW-C illustrated the presence of second and third interdentrite phases, as well as a decreased matrix content compared with that of Mo-C. According to X-ray mappings and spot analysis, ID1 in Mo-C is depleted in Co and enriched in Mo, and, similarly, in W-C, ID1 and ID2 are progressively enriched in W and depleted in Co. However, Cr seemed to be homogeneously distributed in all phases. In contrast, Cr was unevenly distributed in the matrix, and ID2 and ID3 were unevenly distributed in MoW-C, while the Mo and W contents progressively increased in ID1, ID2, and ID3 compared with the matrix. As the temperature decreased during solidification, the dendrites (primary γ) were solidified first, while the remaining molten alloy was pushed in the interdendritic regions and later solidified in the ID phase. The melt in the interdendritic region was enriched in alloying elements due to segregation-in Mo, and/or W, Nb (in the case of W-C)-and C due to carbide formation.[31] These findings were consistent with previous data[45] and should be attributed to differences in the diffusion parameters of alloying elements to the γ-fcc phase, solubility in the solid-state, and other thermodynamic data.[31]

The lower modulus of elasticity (Table 4) in the cast groups may be associated with the presence of extensive porosity (Fig. 1), which significantly decreased the bearing cross-sectional area from the nominal cross-sectional area

Table 3. Indicative elemental compositions of different phases present in cast groups after EDS spot analysis (n=1)

Spot Analysis	Co	Cr	Mo	W	Si	Nb	Ga
Mo-C							
Matrix	61.4(3.7)	31.0(1.9)	6.6(0.6)		0.9(0.1)		
ID1	52.6(3.3)	32.5(2.1)	13.7(1.2)		1.0(0.2)		
W-C							
Matrix	63.1(4.7)	26.5(2.0)		9.3(0.9)	0.9(0.2)		
ID 1	58.9(4.3)	28.3(2.1)		11.1(1.0)	1.3(0.2)	0.2(0.1)	
ID 2	43.9(3.2)	27.0(2.0)		19.2(1.6)	2.3(0.3)	7.3(0.8)	
MoW-C							
Matrix	65.6(5.0)	22.8(1.8)	2.9(0.4)	5.8(0.6)	0.3(0.1)		2.4(0.3)
ID 1	59.1(4.4)	23.9(1.8)	5.6(0.6)	7.2(0.7)	0.9(0.2)		3.1(0.4)
ID 2	49.2(3.7)	28.0(2.2)	9.9(1.1)	9.4(0.9)	0.7(0.1)		2.6(0.4)
ID 3	43.0(3.2)	19.3(1.5)	18.5(1.9)	15.0(1.3)	2.3(0.3)		1.6(0.31)

Error (3-sigma) values calculated automatically from quantitative analysis shown in parentheses. Three-sigma rule indicates level of accuracy, implying that mean value falls within the range (mean value − 3-sigma − mean value + 3-sigma) with 99.7% probability.

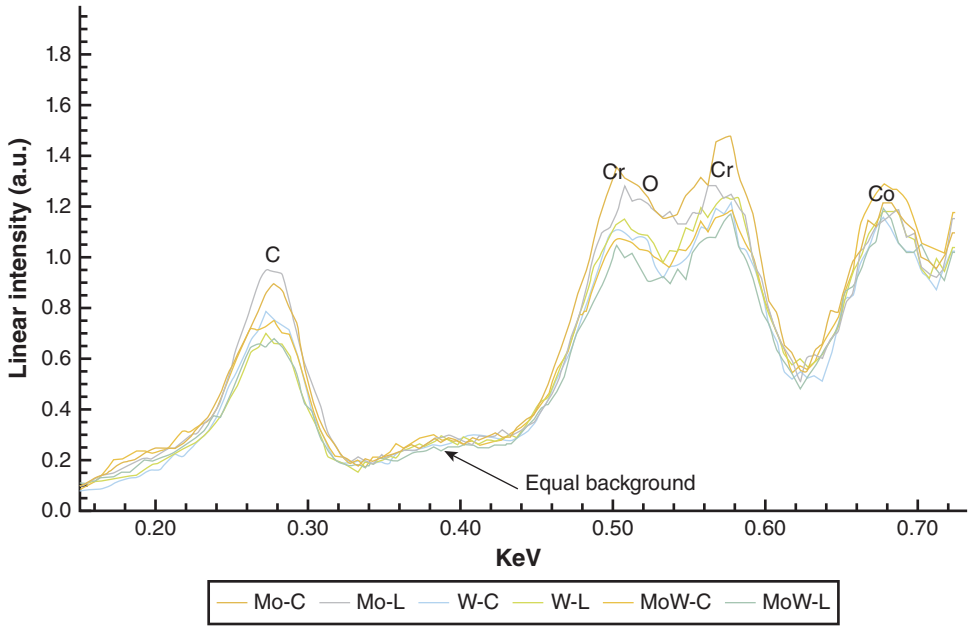

Figure 6. Overlapping energy dispersive X-ray spectra of low-energy region from all groups tested. All spectra have equivalent backgrounds.

Table 4. Mean ±standard deviation values with statistical outcomes of groups tested (n=10)

	Martens Hardness (HM) (N/mm^2)		Elastic Index η_{IT} (%)		Bending Modulus (E_b) (GPa)	
	C	L	C	L	C	L
Mo	3189 ±116^{A1}	3390 ±90^{A2}	19.2 ±0.6^{A1}	20.6 ±0.4^{A2}	178 ±17^{A1}	223 ±31^{A2}
W	2878 ±34^{B1}	3633 ±61^{B2}	17.2 ±0.7^{B1}	20.9 ±0.3^{A2}	183 ±17^{A1}	244 ±36^{A2}
MoW	2601 ±94^{C1}	3122 ±104^{C2}	16.8 ±0.3^{B1}	19.0 ±0.3^{B2}	170 ±25^{A1}	241 ±15^{A2}

Superscripts indicate statistical comparisons with uppercase letters for columns and numbers for rows within each alloy type.

measured using digital calipers. Compared with their cast counterparts, all the alloy types exhibited significantly higher HM values. The elastic index was indicative of the ductility of an alloy, and the higher the elastic index, the more brittle the material. Thus, the SLM groups were more brittle than the cast groups. Given that different factors, such as the carbide content and microstructure residual stresses, contribute to the mechanical properties of Co-Cr alloys,[24,27,28,39] only general approaches can be established because of the possible contributions of these factors to the findings. Low-KeV analysis revealed that the C content was higher in the Mo-C and Mo-L alloys among all the alloys tested, which probably indicates that an increased carbide content is the basic hardening mechanism for Co-Cr alloys. This may explain the higher HM values of Mo-C among the cast alloys, although Mo-L had a lower HM than W-L. However, the HM and η_{IT} of the SLM alloys included the completely unknown influence of residual stresses, which may have a profound effect on these properties.

The clinical implications of these findings are interesting for both clinicians and manufacturers, implying that, independently of alloy formulation, SLM has

significant advantages over conventional casting. The main issue of porosity in cast Co-Cr alloys was that it was independent of the alloy type and was eliminated only by the SLM process. This minimized the adverse effects of porosity on the mechanical properties[20] and susceptibility to crevice and pitting corrosion associated with surface irregularities.[4,33] The corrosion resistance was further enhanced by the microstructure, where the elemental segregation was eliminated in SLM structures. Previous studies have reported that SLM materials have lower ionic release[4,35] and more favorable electrochemical properties[34,43] and biocompatibility[3,35,36] than cast materials.

Limitations of this study included that the tested alloys had similar but not identical elemental compositions to that of Dentaurum. Therefore, the alloys and manufacturing processes cannot be strictly considered independent variables. The findings of this study indicated that SLM should be considered over traditional casting, particularly in terms of the more advantageous porosity, microstructure, and mechanical properties of SLM-fabricated Co-Cr alloys.

CONCLUSIONS

Based on the findings of this in vitro study, the following conclusions were drawn:

1. The gross porosity developed during conventional casting is independent of the alloy type.
2. SLM eliminates internal porosity and provides a uniform microstructure for all 3 alloy types tested.
3. SLM significantly improved the mechanical properties (**HM**, η_{IT}, and E_b) of all 3 Co-Cr alloys tested over those obtained with conventional casting.

REFERENCES

1. Haynes E. Alloys of cobalt with chromium and other metals. *J Ind Eng Chem.* 2002;5:189–191.
2. Al Jabbari YS. Physico-mechanical properties and prosthodontic applications of Co-Cr dental alloys: A review of the literature. *J Adv Prosthodont.* 2014;6:138–145.
3. Fu W, Liu S, Jiao J, et al. Wear resistance and biocompatibility of Co-Cr dental alloys fabricated with CAST and SLM techniques. *Materials (Basel).* 2022;15.
4. Al Jabbari YS, Karavoltsos S, Kokkinos C, et al. Electrochemical characterization of three types of Co-Cr based alloys manufactured by casting and selective laser melting according to ISO 10271. *Dent Mater.* 2022;38:1162–1172.
5. Viennot S, Dalard F, Lissac M, Grosgogeat B. Corrosion resistance of cobalt-chromium and palladium-silver alloys used in fixed prosthetic restorations. *Eur J Oral Sci.* 2005;113:90–95.
6. Wataha JC. Alloys for prosthodontic restorations. *J Prosthet Dent.* 2002;87:351–363.
7. Marti A. Cobalt-base alloys used in bone surgery. *Injury.* 2000;31:18–21.
8. West Conshohocken, PA, USA: ASTM,; 2018.
9. ISO 6871. Dental base metal alloys. International Organization for Standardization. Part 1: Cobalt-based alloys. 1st ed. 1987.
10. ISO 6871–1. Dental base metal alloys. International Organization for Standardization. Part 1: Cobalt-based alloys. 1st ed. 1994.
11. ISO 9693. Dentistry — Compatibility testing for metal-ceramic and ceramic-ceramic systems. Geneva: International Organization for Standardization,; 2019.
12. ISO:22674. Dentistry-Metallic materials for fixed and removable restorations and appliances. International Organization for Standardization,; 2016.
13. van Noort R. The future of dental devices is digital. *Dent Mater.* 2012;28:3–12.
14. Barucca G, Santecchia E, Majni G, et al. Structural characterization of biomedical Co-Cr-Mo components produced by direct metal laser sintering. *Mater Sci Eng C Mater Biol Appl.* 2015;48:263–269.
15. Ko KH, Kang HG, Huh YH, et al. Effects of heat treatment on the microstructure, residual stress, and mechanical properties of Co-Cr alloy fabricated by selective laser melting. *J Mech Behav Biomed Mater.* 2022;126:105051.
16. Wai Cho HH, Takaichi A, Kajima Y, et al. Effect of post-heat treatment cooling conditions on microstructures and fatigue properties of cobalt chromium molybdenum alloy fabricated through selective laser melting. *Metals.* 2021;11.
17. Koutsoukis T, Zinelis S, Eliades G, et al. Selective laser melting technique of Co-Cr dental alloys: A review of structure and properties and comparative analysis with other available techniques. *J Prosthodont.* 2015;24:303–312.
18. Ucar Y, Akova T, Akyil MS, Brantley WA. Internal fit evaluation of crowns prepared using a new dental crown fabrication technique: laser-sintered Co-Cr crowns. *J Prosthet Dent.* 2009;102:253–259.
19. Oyague CR, Lynch CD, Turrion AS, et al. Misfit and microleakage of implant-supported crown copings obtained by laser sintering and casting techniques, luted with glass-ionomer, resin cements and acrylic/urethane-based agents. *J Dent.* 2013;41:90–96.
20. Dharmar S, Rathnasamy RJ, Swaminathan TN. Radiographic and metallographic evaluation of porosity defects and grain structure of cast chromium cobalt removable partial dentures. *J Prosthet Dent.* 1993;69:369–373.
21. Eisenburger M, Addy M. Radiological examination of dental castings – A review of the method and comparisons of the equipment. *J Oral Rehabil.* 2002;29:609–614.
22. Kazantseva NV, Ezhov IV, Davydov DI, Merkushev AG. Analysis of structure and mechanical properties of Co–Cr–Mo alloy obtained by 3D printing. *Phys Met Metallogr.* 2020;120:1172–1179.
23. Takaichi A, Kajima Y, Kittikundecha N, et al. Effect of heat treatment on the anisotropic microstructural and mechanical properties of Co-Cr-Mo alloys produced by selective laser melting. *J Mech Behav Biomed Mater.* 2020;102:103496.
24. Hassani FZ, Ketabchi M, Bruschi S, Ghiotti A. Effects of carbide precipitation on the microstructural and tribological properties of Co–Cr–Mo–C medical implants after thermal treatment. *J Mater Sci.* 2016;51:4495–4508.
25. Yoda K, Suyalatu, Takaichi A, et al. Effects of chromium and nitrogen content on the microstructures and mechanical properties of as-cast Co-Cr-Mo alloys for dental applications. *Acta Biomater.* 2012;8:2856–2862.
26. Rodrigues WC, Broilo LR, Schaeffer L, et al. Powder metallurgical processing of Co-28%Cr-6%Mo for dental implants: Physical, mechanical and electrochemical properties. *Powder Technol.* 2011;206:233–238.
27. Ayyildiz S, Soylu EH, Ide S, et al. Annealing of Co-Cr dental alloy: effects on nanostructure and Rockwell hardness. *J Adv Prosthodont.* 2013;5:471–478.
28. Linn Htat H, Takaichi A, et al. Influence of stress-relieving heat treatments on the efficacy of Co-Cr-Mo-W alloy copings fabricated using selective laser melting. *J Prosthodont Res* 2023.
29. Lewis AJ. Microporosity in casting alloys. *Aust Dent J.* 1975;20:161–166.
30. van Noort R, Lamb DJ. A scanning electron microscope study of Co-Cr partial dentures fractured in service. *J Dent.* 1984;12:122–126.
31. Yamanaka K, Mori M, Sato K, Chiba A. Characterisation of nanoscale carbide precipitation in as-cast Co-Cr-W-based dental alloys. *J Mater Chem B.* 2016;4:1778–1786.
32. Al Jabbari YS, Koutsoukis T, Barmpagadaki X, Zinelis S. Metallurgical and interfacial characterization of PFM Co-Cr dental alloys fabricated via casting, milling or selective laser melting. *Dent Mater.* 2014;30:e79–e88.
33. Munoz AI, Mischler S. Effect of the environment on wear ranking and corrosion of biomedical CoCrMo alloys. *J Mater Sci Mater Med.* 2011;22:437–450.
34. Xin XZ, Xiang N, Chen J, et al. Corrosion characteristics of a selective laser melted Co-Cr dental alloy under physiological conditions. *J Mater Sci.* 2012;47:4813–4820.
35. Xin XZ, Xiang N, Chen J, Wei B. In vitro biocompatibility of Co-Cr alloy fabricated by selective laser melting or traditional casting techniques. *Mater Lett.* 2012;88:101–103.
36. Hedberg YS, Qian B, Shen Z, et al. In vitro biocompatibility of CoCrMo dental alloys fabricated by selective laser melting. *Dent Mater.* 2014;30:525–534.
37. Al Jabbari YS, Barmpagadaki X, Psarris I, Zinelis S. Microstructural, mechanical, ionic release and tarnish resistance characterization of porcelain fused to metal Co-Cr alloys manufactured via casting and three different CAD/CAM techniques. *J Prosthodont Res.* 2019;63:150–156.

38. Roberts HW, Berzins DW, Moore BK, Charlton DG. Metal-ceramic alloys in dentistry: a review. *J Prosthodont*. 2009;18:188–194.
39. Dimitriadis K, Foteinidis G, Kosarli M, et al. Microstructure and mechanical properties of Co-Cr alloy fabricated by selective laser melting technology for removable partial denture frameworks. *J Mater Eng Perform* 2022.
40. Jang KS, Youn SJ, Kim YS. Comparison of castability and surface roughness of commercially pure titanium and cobalt-chromium denture frameworks. *J Prosthet Dent*. 2001;86:93–98.
41. Sandu L, Faur N, Bortun C. Finite element stress analysis and fatigue behavior of cast circumferential clasps. *J Prosthet Dent*. 2007;97:39–44.
42. Sedlaček M, Zupančič K, Šetina Batič B, et al. Influence of precipitation hardening on the mechanical properties of Co-Cr-Mo and Co-Cr-W-Mo dental alloys. *Metals*. 2023;13.
43. Wei W, Zhou Y, Liu W, et al. Microstructural characterization, mechanical properties, and corrosion resistance of dental Co-Cr-Mo-W alloys manufactured by selective laser melting. *J Mater Eng Perform*. 2018;27:5312–5320.
44. Im H-T, Kim DH, Kim YD, et al. Effect of phase transformation on the mechanical properties of the Co-Cr-Mo alloy fabricated by selective laser melting. *Mater Charact*. 2022;186.
45. Kim HR, Jang SH, Kim YK, et al. Microstructures and mechanical properties of Co-Cr dental alloys fabricated by three CAD/CAM-based processing techniques. *Materials (Basel)*. 2016;9.
46. Li KC, Prior DJ, Waddell JN, Swain MV. Microstructure, phase content, and thermal stability of a cast Co–Cr dental alloy after porcelain sintering cycles using electron backscatter diffraction. *J Mater Res*. 2015;30:2188–2196.
47. Goldstein J, Newbury D, Echlin P, et al. Chapter 10 Special topics in Electron Beam X-ray Microanalysis. Scanning Electron Microscopy and X-Ray Microanalysis. 3rd ed.,. New York: Springer,; 2003:499–509.
48. ISO:14577-1. Metallic materials-Instrumented indentation test for hardness and materials parameters. Geneva: International Organization for Standardization,; 2002.

Corresponding author:
Dr Youssef S. Al Jabbari
King Saud University College of Dentistry
P.O. Box 60169
Riyadh 11545
SAUDI ARABIA
Email: yaljabbari@ksu.edu.sa

CRediT authorship contribution statement

Youssef S. Al Jabbari: PI and research grant applicant and recipient, Conceptualization, Methodology, Investigation, Writing - review and editing. **Konstantinos Dimitriadis:** Investigation, Formal analysis, Visualization, Writing- original draft preparation. **Aref Sufyan:** Investigation, Formal analysis, Writing- original draft preparation. **Spiros Zinelis:** Conceptualization, Methodology, Investigation, Visualization, Writing - review and editing.

https://doi.org/10.1016/j.prosdent.2024.06.015